Published in final edited form as:

Cancer Res. 2018 July 15; 78(14): 3969–3981. doi:10.1158/0008-5472.CAN-18-0388.

Evidence of inter-tissue differences in the DNA damage response and the pro-oncogenic role of NFκB in mice with disengaged BRCA1-PALB2 interaction

Amar Hekmat Mahdi[1,2,*], **Yanying Huo**[1,2,*], **Yongmei Tan**[1,2,3], **Srilatha Simhadri**[1,4], **Gabriele Vincelli**[1,2], **Jie Gao**[3], **Shridar Ganesan**[1,4], and **Bing Xia**[1,2]

[1]Rutgers Cancer Institute of New Jersey, Rutgers Robert Wood Johnson Medical School, 195 Little Albany Street, New Brunswick, NJ 08903

[2]Department of Radiation Oncology, Rutgers Robert Wood Johnson Medical School, 195 Little Albany Street, New Brunswick, NJ 08903

[3]Stomatological Hospital of Guangzhou Medical University, 31 Huangsha Road, Guangzhou 510140, P.R. China

[4]Department of Medicine, Rutgers Robert Wood Johnson Medical School, 195 Little Albany Street, New Brunswick, NJ 08903

Abstract

The BRCA1-PALB2-BRCA2 axis plays an essential role in DNA homologous recombination repair (HRR), defect in which drives genome instability and cancer development. How cells with defects in this pathway respond to DNA damage in vivo and how tumors develop from these cells remain poorly defined. Here we analyzed several aspects of the DNA damage response in multiple tissues of *Palb2* mutant mice in which the interaction between PALB2 and BRCA1 is disengaged. Without any challenge, the mutant mice showed increased endogenous DNA damage. Following ionizing radiation (IR), the mutant mice displayed higher levels of DNA breaks and stronger induction of p53 and p21, but continued DNA synthesis, reduced apoptosis, and accelerated tumor development. The differences in p21 induction, DNA synthesis and apoptosis between wild-type and mutant mice were substantially more pronounced in the mammary gland than in the intestine, suggesting a potential contributing factor to the increased risk and the tissue specificity of *BRCA*/*PALB2*-associated tumor development. Moreover, the mutant mice showed higher levels of reactive oxygen species (ROS) and constitutive activation of NFκB, an anti-apoptotic transcription factor inducible by both DNA damage and oxidative stress. Treatment of the mutant mice with an inhibitor of NFκB reactivated apoptosis and delayed tumor development following radiation. Thus, our results also suggest a pro-survival and pro-oncogenic role of NFκB in *PALB2* mutant cells.

Corresponding author: Bing Xia, Rutgers Cancer Institute of New Jersey, 195 Little Albany Street, New Brunswick, NJ 08903. xiabi@cinj.rutgers.edu.

*These authors contributed equally to this work.

Current address for A.H. Mahdi: Department of Physiology, College of Medicine, Al-Mustansiriyah University, Baghdad, Iraq

The authors declare no conflicts of interest.

Keywords

PALB2; BRCA1; BRCA2; NFκB; p53; thymic lymphoma

Introduction

PALB2 is a tumor suppressor that functions in conjunction with BRCA1 and BRCA2 in the DNA damage response and maintenance of genome integrity, impairment of which is a major driver of cancer development (1). In particular, PALB2 controls the intra-nuclear localization of BRCA2 and links BRCA1 and BRCA2 in homologous recombination (HR)-based repair of DNA double strand breaks (DSBs) (2–4). Consistent with its biochemical function as a controller of BRCA2 and a linker between BRCA1 and BRCA2, PALB2 itself is a tumor suppressor with disease phenotypes similar to both BRCA1 and BRCA2 and nearly identical to BRCA2 (5). Specifically, heterozygous (or monoallelic) germline mutations in *PALB2* increase the risk of cancer development in the breast, ovary and pancreas, whereas biallelic mutations in the gene cause Fanconi anemia (FA) (5). The breast cancer risk of *PALB2* mutation carriers approach that of *BRCA2* carriers (6), and the phenotypes of FA patients with biallelic *PALB2*/*FANCN* and *BRCA2*/*FANCD1* mutations are virtually identical, with unusual severity and hallmark features of “embryonal” cancers such as medulloblastoma and Wilm’s tumor (7–9).

Conventional knockout of each of *Brca1*, *Brca2* and *Palb2* genes in the mouse leads to embryonic lethality which can be partially rescued by co-deletion of *Trp53* (10–12). Tissue-specific knockout of each gene in the mammary gland results in tumor formation with long latency, with most of the tumors tested containing somatic mutations in *Trp53* (13,14). Co-ablation of *Trp53* in the same tissue or even a *Trp53* heterozygous background accelerates mammary tumor development (13,15–17). Therefore, p53 is a barrier to cell proliferation and tumorigenesis following the loss of BRCA and PALB2 proteins, and an inactivation of p53 or its pathway may be a prerequisite for their associated tumorigenesis. Indeed, practically all human *BRCA1* breast cancers harbor somatic mutations or deletions in *TP53* (18). There are also reports suggesting higher *TP53* mutation rates in *BRCA2* and *PALB2* mutant breast cancers than in sporadic cancers, albeit the data are less conclusive.

In addition to p53, another major transcription factor, NFκB, has recently been implicated in *BRCA1*-associated breast cancer development. NFκB regulates a variety of genes with diverse functions, with its overall activity being pro-inflammatory, anti-apoptotic, pro-survival and pro-oncogenic (19,20). NFκB can be activated by canonical, non-canonical or atypical pathways (19). The canonical and atypical pathways mainly involve p65 (RelA) and p50, whereas non-canonical pathway involves another set of components, p68 (RelB) and p52. Interestingly, NFκB p52/RelB is persistently activated in a subset of luminal progenitors in the mammary gland of *BRCA1* (heterozygous) mutation carriers and in BRCA1-depleted cells (21). Moreover, blockade or inactivation of RANKL/RANK signaling, an inducer of the non-canonical NFκB pathway, inhibited the proliferation and expansion of *BRCA1* heterozygous mammary progenitors as well as mammary tumor

formation in *Brca1* conditional knockout mouse models (21–23), suggesting that NFκB plays a pro-oncogenic role in *BRCA1*-associated tumorigenesis.

The virtually identical tumor phenotypes of human FA-D1 (*BRCA2*) and FA-N (*PALB2*) patients and the highly similar tumor spectra of *PALB2* and *BRCA2* heterozygous carrier families strongly indicate that the tumor suppressive function of BRCA2 largely depends on its association with PALB2. In both BRCA1 and BRCA2, patient-derived missense mutations that disrupt their interaction with PALB2 have been identified and shown to abrogate their HR function (2,3,24). Very recently, we reported a breast cancer family segregating a missense mutation in PALB2 that disrupt its interaction with BRCA1 and completely abrogates its HR activity (25). These findings suggest that intact BRCA1-PALB2-BRCA2 interactions are required for tumor suppression. This notion is supported by a recent study showing increased tumor development in a mouse strain with a hypomorphic mutation (G25R) in BRCA2 that partially disrupts its binding to PALB2 (26). However, the importance of the BRCA1-PALB2 interaction in tumor suppression has not been directly tested.

To overcome the embryonic lethality of conventional *Palb2* knockout, we previously generated a *Palb2* knockin mouse strain with a 3-aa mutation (LKK→AAA) in the N-terminal coiled-coil domain that abrogates BRCA1 binding (27). Homozygous mutant mice were viable and did not show any overt abnormality, except slightly smaller body size (unpublished) and a moderate male-specific fertility defect (27). This strain allows for exploration of the role of PALB2 and the BRCA1-PALB2 interaction in different tissues, affording us an opportunity to gain insights into the in vivo mechanisms and tissue specificity of *PALB2*-associated tumorigenesis. In the current study, we analyzed several aspects of the DNA damage response, i.e. DNA repair, DNA synthesis, p53 induction and apoptosis, in multiple tissues of the mutant mice after ionizing radiation (IR), and monitored tumor incidence in these mice following IR. In addition, we also tested the role of NFκB in radiation-induced apoptosis and tumor development in these mice.

Materials and Methods

Mice

Generation of the $Palb2^{CC6}$ (LKK-AAA) mutant strain was described before (27). The strain was backcrossed to C57BL/6 background for 6 generations before being used in this study. C57BL/6 mice were used as wt control. Genotyping was carried out as described (27). All animal work was approved by the Institutional Animal Care and Use Committee (IACUC) of the Rutgers Robert Wood Johnson Medical School.

Gamma radiation

For studying DNA damage response, mice were treated with a single dose of 3 Gy of whole body γ-radiation at the age of 8 weeks. For studying tumor development, mice were treated with 2 Gy of whole body radiation once a week for 3 weeks, starting from 8 weeks of age. Radiation was delivered from a Cesium137 source (Gammacell 40 Exactor, Best Theratronics Ltd., Ottawa, Ontario, Canada) at a dose rate of 0.97 Gy/min.

5-Bromo-2′-deoxyuridine (BrdU) labeling

BrdU was purchased from Sigma-Aldrich and dissolved in phosphate-buffered saline (PBS). Mice were injected intraperitoneally at a dose of 100 mg/kg, and the labeling was for 30 min before tissue collection at each time point.

Immunohistochemistry (IHC)

Tissues were fixed in 10% buffered formalin solution for 24 hr and then transferred to 70% ethanol prior to further processing. Paraffin-embedded block production and sectioning were conducted by The Histopathology Shared Resources of Rutgers Cancer Institute of New Jersey. IHC was performed on 5 μm sections as described before (27). The following antibodies were used: γH2AX-pSer139 (EMD Millipore, #07-164, 1:200 dilution), p53 (Leica Biosystems, NCL-p53-CM5p, 1:1000 dilution), p21 (Santa Cruz, sc-6246, 1:50 dilution), BrdU (BD Biosciences, #347580, 1:100 dilution) and NFκB p65 (GeneTex, GTX50371, 1:200).

Terminal deoxynucleotidyltransferase dUTP nick end labeling (TUNEL) assay

Staining was performed on 5 μm sections using the DeadEnd™ Fluorometric TUNEL System (Promega) according to the manufacturer's instructions.

Quantification of IHC and TUNEL results

At least 5–7 representative fields at 40X magnification were counted. A minimum of 200–300 cells from each slide/condition were scored for each genotype. All experiments were performed for at least 3 times (unless otherwise indicated), each with 2 mice per genotype per time point.

ROS measurement

MEFs were generated following standard procedures and cultured in Dulbecco's modified Eagle's medium (DMEM) supplemented with 10% heat-inactivated fetal bovine serum (FBS) and 1 X penicillin-streptomycin (Pen-Strep) at 37 °C in a humidified incubator with 5% CO_2. ROS levels were measured as described before (28). Briefly, cells grown in 6-well plates were washed with PBS and then incubated with fresh phenol red-free medium containing 25 μM DCF-DA (2′,7′-dichlorofluorescein diacetate) (Sigma, catalog no. D6883) at 37°C for 20 min. Cells were trypsinized and analyzed by flow cytometry with excitation at 488 nm and emission at 515 to 545 nm.

Western blotting

Mouse embryonic fibroblasts (MEFs) were lysed with NETNG-400 (400mM NaCl, 1 mM EDTA, 20 mM Tris-HCl [pH7.5], 0.5% Non-Idet P-40, and 10% glycerol) with Complete® protease inhibitor cocktail (Roche). Tissues were homogenized in the same buffer and sonicated. Samples were resolved on 4–12% Tris-glycine SDS-polyacrylamide gels and transferred to a nitrocellulose membrane (0.45 micron, Bio-Rad). The primary antibodies used were as follows: NFκB p65 (Santa Cruz, #sc109, at 1:200, and Abcam, #ab16502, at 1:1000), and β-Actin (Santa Cruz, #Ac-15 at 1:5,000). The secondary antibodies used were

Amersham ECL HRP Conjugated Antibodies (GE Healthcare Life Sciences). Blots were developed using Immobilon Western Chemiluminescent HRP Substrate (EMD Millipore).

TPCA-1 administration

Mice at 8 weeks of age were treated with intraperitoneal injection of the TPCA-1 (2-[(aminocarbonyl)amino]-5-(4-fluorophenyl)-3-thiophenecarboxamide) (Selleckchem), a selective inhibitor of IKK2 (IKKβ), at 20 mg/kg body weight, twice at 12 hr apart. TPCA-1 was given in a vehicle consisting of 0.9% DMSO, 7% dimethylacetoacetamide (DMA) and 10% Cremophor EL (both from Sigma-Aldrich) in PBS. Radiation was delivered 2 hr after the 2nd TPCA-1 injection.

Statistical analyses

For IHC, TUNEL and ROS results, p values were calculated with two-tailed student's *t*-test using Microsoft Excel. For Kaplan-Meier survival curves, p value was determined with log-rank analysis using GraphPad Prism7. P values of ≤0.05 were considered significant.

Results

Increased endogenous DNA damage and reduced DSB repair capacity in *Palb2* mutant mice

To assess the importance of the interaction between PALB2 and BRCA1 for the repair of DNA damage in vivo, we analyzed the amount of endogenous DSBs in the mammary gland and intestine of wild-type (wt) and the *Palb2* knockin mutant females by immunohistochemistry (IHC), with an antibody against phosphorylated histone H2AX (γH2AX), a marker for DSBs. In the mutant mice, discrete γH2AX foci were found in approximately 40% of mammary epithelial cells, among which about 10% contained 4–6 foci (in a single focal plane) (Fig. 1A,B). In comparison, γH2AX foci were detected in only 17% of mammary epithelial cells in the wt mice, and none of the cells contained more than 3 foci. In the intestine, positive γH2AX staining was mostly found in the crypt (Fig. 1C), the stem cell compartment. Overall, less than 10% of cells in the intestinal crypts of wt mice were positive for γH2AX foci, whereas the number was about 40% in the mutant mice (Fig. 1D). These observations indicate that the BRCA1-PALB2 interaction is required for the efficient repair of endogenous DSBs or the prevention of DSB formation during normal DNA metabolism. We then assessed the capacity of DSB repair in these mice by monitoring γH2AX foci clearance at different time points after IR (3 Gy). As expected, a dramatic induction of γH2AX foci was observed in both the mammary gland and the intestine at 30 min after IR, and the extent of induction was similar in the wt and mutant mice (Fig. 1A–D). However, the rate of γH2AX foci disappearance in both tissues was slower in the mutant mice, indicating that the binding between BRCA1 and PALB2 is important for the repair of DSBs in vivo.

Continued proliferation and resistance to apoptosis in *Palb2* mutant mice after irradiation

To test whether abrogation of the PALB2-BRCA1 interaction would impact the response of cells to DNA damage, we first measured of DNA synthesis in wt and mutant mice after IR. The mice were labeled with 5-bromo-2-deoxyuridine (BrdU) at different time points and its

incorporation in the mammary gland and intestine were analyzed by IHC. In wt mice, the number of BrdU-positive cells decreased in both tissues after IR (Fig. 2A–D), indicative of a halt of DNA synthesis in cells already in the S phase at the time of radiation (intra-S phase checkpoint) and/or an inhibition of new S phase entry (G1/S checkpoint). In comparison, no decrease in BrdU-positive cells were observed in either tissue of the mutant mice (Fig. 2A–D), despite the fact that they contained more DNA damage (Fig. 1). Strikingly, the number of BrdU-positive cells in the mutant mammary gland at 6 hr post IR was almost 4 times as high as its baseline level before IR (Fig. 2B). Although this is reminiscent of the S-phase checkpoint defect in PALB2-depleted cells we reported before (2), it should be noted that an S-phase checkpoint defect would simply maintain the level of DNA synthesis in a given cell already in the S phase at the time of DNA damage. Therefore, the large increase in the number of BrdU-positive cells in the mutant mammary gland, which may reflect a large, synchronized wave of S-phase entry “orchestrated” by IR, is likely due to a novel mechanism that remains to be elucidated.

Next, we determined the extent of apoptosis in the two tissues using the terminal deoxynucleotidyl transferase end labeling (TUNEL) assay. Before radiation, small and similar numbers of apoptotic cells were detected in the mammary gland of both wt and mutant mice (4% vs 3%, respectively) (Fig. 2E,F). In comparison, larger numbers of apoptotic cells were found in the intestines of both wt and mutant mice, although the number in the mutant intestine was smaller than that in its wt counterpart (Fig. 2G,H). After radiation, increased apoptosis was detected in both tissues of both genotypes. Notably, the increase was substantially less pronounced in the mutant mammary gland (Fig. 2F). At 6 hr after radiation, the number of apoptotic cells had increased by approximately 5 fold (from ~4% to ~20%) in the wt mammary gland, whereas a much more muted 2-fold increase (from ~3% to ~6%) was observed in the mutant tissue. At the same time, apoptotic cells in the intestine increased by approximately 1.6 and 2 fold, respectively, in the wt and mutant mice (Fig. 2H). At both 6 and 24 hr post IR, the levels of apoptosis were lower in both the mammary gland and the intestine in the mutant mice, and the differences were larger in the mammary gland (Fig. 2G,H). Thus, an unperturbed interaction between BRCA1 and PALB2 is critical for the suppression of DNA synthesis/cell proliferation and normal execution of apoptosis after DNA damage.

Higher induction of p53 and p21 in *Palb2* mutant mice after DNA damage

Given the well-established role of p53 in promoting cell cycle arrest and apoptosis after DNA damage, we examined its levels by IHC. Without radiation, the mammary gland in both wt and mutant mice stained negative (Fig. 3A). At 6 hr after radiation, p53 induction was observed in a subset of cells in both wt and mutant mammary epithelia, with the mutant tissue showing both stronger straining signals and more positive cells (Fig. 3A,B). Compared with the mammary gland, p53 induction was much more robust in the intestine in both wt and mutant mice (Fig. A,B). Again, the induction was stronger in the mutant than the wt tissue. To assess p53 activity, we stained the tissues for its major target, p21. Consistent with the difference in p53, the induction of p21 was also stronger in the mutant mice (Fig. 3C). Quantification of positive cells showed a much more extensive (occurring in more cells) induction of p21 in the mutant mammary gland than in its wt counterpart,

especially at 6 hr after IR, where the difference was more than 15 fold (24% vs 1.5%) (Fig. 3D). In the intestine, p21 was induced in more cells than in the mammary gland in both genotypes (Fig. 3C,D). The induction was again more extensive in the mutant tissue, and the difference between the two genotypes was less pronounced than that in the mammary gland. Collectively, these results demonstrate a more robust induction of p53 and p21 in the mutant mice after DNA damage and a profound difference between p21 induction in wt and mutant mammary glands.

Accelerated tumor development in *Palb2* mutant mice after radiation

To assess the role of the BRCA1-PALB2 interaction in tumor suppression, we monitored tumor development in the mice after radiation (3 × 2 Gy with one week interval, starting from 8 weeks of age). Compared with wt mice, mutant animals showed vastly accelerated tumor development (median latency 255 days versus >700 days, respectively) (Fig. 4A). By the end of the 700-day observation period, 44 of 48 (92%) mutant animals had developed tumors, three of the rest had died of unknown reasons, and one remained alive; in contrast, only 14 of 50 (28%) wt animals had developed tumors, 4 (8%) died of unknown reasons, and 31 (62%) were alive. Therefore, the PALB2-BRCA1 interaction is critical for the suppression of radiation-induced tumorigenesis. No significance differences in overall survival were observed between males and females of either genotype (Fig. 4B). In both wt and mutant mice, the majority of tumors were thymic lymphoma (Fig. 4C). Among the wt females, two developed mammary tumors and one developed ovarian cancer. In comparison, none of the mutant females developed mammary tumors and two of them developed ovarian cancer.

DNA damage response in the thymus of wt and *Palb2* mutant mice

With thymic lymphoma being the major tumor type in both wt and mutant animals, we analyzed the same parameters as above to understand the DNA damage response in the thymus. Before radiation, the mutant thymus already contained more γH2AX positive cells (Fig. 5A). At 30 min after IR, γH2AX was dramatically induced in all thymic cells of both genotypes. By 3 hr after IR, the overall staining intensity had decreased moderately in both wt and mutant tissues, although virtually all cells were still positive. At these two time points, the staining pattern and intensity of the wt and mutant tissues were indistinguishable. By 6 hr after IR, γH2AX staining had decreased substantially in both wt and mutant tissues, with patches of cells having become negative and the rest of cells showing varying staining patterns and intensities. The overall staining intensity appeared to be slightly stronger in the mutant tissue, although the difference was hard to quantify. These observations indicate that a DSB repair defect also exists in the mutant thymus. Next, we examined p53 induction, BrdU incorporation and apoptosis by IHC and TUNEL assays. As shown in Fig. 5B and C, the mutant thymus contained more p53-positive cells after IR but also more cells actively incorporating BrdU. Moreover, fewer apoptotic cells were found in the mutant thymus both before and after radiation (Fig. 5D,E). These results are consistent with the findings made in the mammary gland and intestine, further indicating a disconnect between the induction of p53 and its ability to induce cell cycle arrest and apoptosis in all 3 tissues analyzed.

Increased reactive oxygen species (ROS) levels in *Palb2* mutant mice

ROS play key roles in diverse cellular signaling pathways exerting significant impact on many aspects of cellular physiology including proliferation and death/survival. Previously, we reported that PALB2 promotes the nuclear accumulation of the master antioxidant transcription factor NRF2 by competitively binding to its negative regulator KEAP1, thereby acting as an antioxidant protein (28). Similarly, BRCA1 has also been reported to possess an NRF2-dependent antioxidant function (29–31). To test if the mutation in PALB2 being studied here affects ROS levels in vivo, we used IHC to measure the levels of 8-oxo-deoxyguanidine (8-oxo-dG), a marker of DNA oxidation, in the same 3 tissues. As depicted in Fig. 6A, stronger staining signals were observed in all 3 tissues of the mutant mice, suggestive of higher ROS levels. Moreover, we generated mouse embryonic fibroblasts (MEFs) from wt and mutant embryos and measured ROS levels in these cells using 2′,7′-dichlorofluorescein diacetate (DCF-DA). Again, results from 3 pairs of MEFs consistently showed substantially higher levels of ROS in the mutant than in the wt cells (Fig. 6B). Note that ROS levels were measured at passage 2, before the mutant MEFs started to undergo senescence after passage 3 (27). Taken together, these results establish increased ROS levels in mutant mice and further suggest that PALB2 and BRCA1, at least in part, may function together to promote cellular antioxidant capacity.

Constitutive activation of NFκB and its anti-apoptotic role in *Palb2* mutant mice

The discrepancy between the higher p53 induction and lower apoptosis levels in the mutant mice led us to hypothesize that p53 transcriptional activity may be either dependent on the BRCA1-PALB2 complex or overcome by another factor. The first possibility was largely ruled out by the efficient p21 induction in the mutant tissues (Fig. 3). Therefore, we surmised that p53 activity may be offset by another factor in the mutant cells. We considered NFκB as a candidate for such a factor for 3 reasons. First, it can be activated by both DNA damage and ROS (32,33). Second, it has well-established anti-apoptotic activity (20). Third, recent studies strongly suggest a pro-oncogenic role of this factor in *BRCA1*-associated tumorigenesis (21–23). Indeed, the level of the NFκB (p65 subunit) was found to be much higher in the mutant MEFs (Fig. 6C). Moreover, IHC analysis of 4 different tissues in the mutant mice consistently showed stronger nuclear NFκB staining than that in the wt mice (Fig. 7A), and western blotting revealed much higher abundance of total NFκB protein in the mutant spleen (Fig. 7B). In addition, p53 was clearly induced in the mutant spleens even without IR challenge (Fig. 7B).

Next, we asked whether inhibition of NFκB could restore radiation-induced apoptosis in the mutant mice. We treated the mice with 2-[(aminocarbonyl)amino]-5-(4-fluorophenyl)-3thiophenecarboxamide (TPCA-1) and tested for apoptosis in the mammary gland, intestine and thymus after IR by TUNEL. TPCA-1 is an inhibitor of IκB kinases (IKKs), which phosphorylate IκB (inhibitor of NFκB) leading to its degradation and, in turn, activation of NFκB. Indeed, TPCA-1 treatment led to increased levels of apoptosis in all 3 tissues of the mutant mice (Fig. 7C–H). At 6 hr after IR, the differences ranged from 5-fold in the mammary gland (33% vs 6.4%, Figs. 7D and 2F) to 3-fold in the intestine (43% vs 14%, Figs. 7F and 2H) and about 2-fold increase in the thymus (79% vs 43%, Figs. 7H and 5E). For the wt mice, TPCA-1 treatment did not produce any major difference in

apoptosis in the intestine and thymus, at least at 6 hr post IR (compare Figs. 2H and 5E with Figs. 7F and 7H, respectively). At the same time, an approximately 2.5-fold reduction of apoptotic cells was observed in the mammary gland of wt mice treated with TPCA-1 (19.4% vs 7.5%, Figs. 2F and 7D), the cause of which remains to be determined. Overall, TPCA-1 treatment more than restored the level of apoptosis in all 3 tissues of the mutant mice tested, as they contained greater numbers of apoptotic cells than did their wt counterparts after treatment (Fig. 7C–H).

Finally, we tested if TPCA-1 treatment could prevent radiation-induced tumor development in the mutant mice. The mice were irradiated as before (3 × 2 Gy with one week intervals, starting from 8 weeks of age), except that half of them were treated with TPCA-1 prior to each dose, and monitored for tumor development. Indeed, TPCA-1-treatment led to a statistically significant, albeit modest, delay of tumor development (Fig. 7I). All tumors in both TPCA-1 untreated and treated mice were thymic lymphoma. Collectively, our findings suggest that cells in the mutant mice are dependent on NFκB for their survival and therefore tumorigenic potential after DNA damage.

Discussion

Since BRCA1 and BRCA2 were cloned in the mid 1990's, there have been a myriad of studies on their molecular functions in a variety of cellular processes such as DNA repair, DNA replication, cell cycle checkpoints, cell division and transcriptional regulation, etc. Also, a large number of conventional and conditional knockout mouse models have been generated for each gene. Additionally, many studies have examined human tumor and, in some cases, normal breast tissue samples from carriers of germline mutations. The same applies to PALB2, although the numbers of studies and models are smaller in absolute terms. These studies have vastly advanced our understanding of the biological functions and genetic mechanisms of these tumor suppressors. However, relatively speaking, there has been a lack of efforts to systematically understand their functions and mechanisms in vivo. As a result, the mechanism behind the tissue specificity and the path of tumor development in *BRCA1/2* and *PALB2* mutation carriers remain poorly defined.

In this study, in attempting to better understand the function of the BRCA1-PALB2 interaction in vivo and the tissue specificity of their associated tumor development, we first compared several aspects of DNA damage response in the mammary gland and intestine of wt and *Palb2* mutant mice with a mutation that disengages the endogenous BRCA1-PALB2 interaction (27). Our results reveal increased levels of endogenous DNA damage and reduced capacity to resolve radiation-induced DNA damage in both tissues in the mutant mice (Fig. 1), demonstrating the important role of PALB2 and the BRCA1-PALB2 interaction in DNA repair in vivo. Following radiation, the levels of p53 and p21 induction were both higher in the mutant mice (Fig. 3); however, both tissues of the mutant mice also showed higher levels of DNA synthesis/proliferation and lower levels of apoptosis than their wt counterparts (Fig. 2). Later, we also conducted similar analyses in the thymus, and similar observations were made (Fig. 5). Overall, within the same mice the 3 tissues showed largely similar response to radiation. However, the differences between wt and mutant mice in p21 induction, BrdU incorporation and apoptosis following radiation were substantially

more pronounced in the mammary gland than in the intestine, implying a potential fundamental difference in BRCA/PALB2-associated DNA damage response between the two tissues, which may contribute to the large difference in the risks of cancer development in the two tissues among mutation carriers.

The tissue specificity of *BRCA*- and *PALB2*-assocated tumorigenesis has proven difficult to model in mice, as homozygous knockout of each gene causes embryonic lethality, whereas heterozygous mice do not show any meaningful tumor phenotypes (10,34,35). Following radiation, *Palb2* mutant mice developed tumors with much shorter latency and much higher penetrance than did wt mice (Fig. 4A), demonstrating the key role of the BRCA1-PALB2 interaction in tumor suppression. However, the majority of tumors were lymphoma in the thymus, with only 8% of females developing mammary and/or ovarian tumors (Fig. 4C). This seemingly “nonspecific” tumor formation may be explained by at least two possible reasons. First, there may be little tissue specificity of the basic tumor suppression function of PALB2. Second, potential tumor development in more clinically relevant tissues may have longer latency than thymic lymphoma after radiation and therefore be preceded by the latter.

In humans, biallelic mutations in *BRCA1* likely cause embryonic lethality in the vast majority of cases, as inferred from the extreme rarity of biallelic mutation carriers. To date, there have been only 3 such cases reported (36–38). For *BRCA2* and *PALB2*, more bilallelic mutation carriers have been reported (even though their mutation frequencies in the general population are lower than that of *BRCA1*), and they almost invariably develop embryonal cancers such as medulloblastoma (brain) and Wilms tumor (kidney) during infancy or early childhood (8,9). Interestingly, a recent report showed for the first time non-Hodgkin lymphoma (NHL) in two patients at ages of 15 and 17 carrying biallelic *PALB2* mutations, one being a truncating mutation and the other an in-frame skipping of exon 6 (39). As this mutation results in a hypomorphic PALB2 protein still able to bind both BRCA1 and BRCA2, the finding indicates that biallelic but relatively mild mutations in *PALB2* can cause lymphoma instead of Fanconi anemia and embryonal cancers. Therefore, lessons from biallelic mutation carriers suggest that the fundamental tumor suppression activity of these proteins is broader than commonly thought and that the tissue specificity of *BRCA*/*PALB2*-associated tumor development in heterozygous mutation carriers may be mainly due to differentials in the rate of loss of heterozygosity (LOH) or the ability of the cells to survive and proliferate after LOH in different tissues.

Finally, a key finding in this study is the lower levels of apoptosis in the mutant mice following radiation despite their having more DNA damage and stronger induction of p53. Compared with wt mice, these mice contain more endogenous DNA damage and ROS (Figs. 1 and 6, respectively), both of which are known inducers of NFκB, a major transcription factor with anti-apoptotic and pro-oncogenic activities. Indeed, stronger NFκB nuclear staining signals were detected in 4 different tissues of the mutant mice (Fig. 7A). Interestingly, the activation of NFκB in the mutant mice was not limited to its nuclear translocation, as the total protein amount of NFκB (p65) was also much higher in both mutant MEFs (Fig. 6C) and the spleen of mutant mice (Fig. 7B). Thus, our data suggest that NFκB may be protecting the mutant cells from p53-induced apoptosis following IR. Remarkably, treatment of mutant mice with TPCA-1 greatly elevated radiation-induced

apoptosis, to levels even higher than that in wt mice (Fig. 7C–H), and modestly delayed radiation-induced tumor development in the mutant mice. Taken together, our findings implicate NFκB in *PALB2*-associated tumorigenesis and suggest that inhibition of NFκB may have the potential to prevent tumor development in *PALB2* mutation carriers much like *BRCA1* mutation carriers. Finally, it should be noted that TPCA-1 has also been shown to inhibit the phosphorylation of another transcription factor, STAT3 (40), which could also contribute to the observed effect. Additional work with more specific inhibitors and genetic ablation of NFκB pathway components are required to further define the precise contribution of NFκB in *PALB2*-associated tumor development.

Acknowledgments

Financial support: National Cancer Institute (R01CA138804 and R01CA188096 to BX)

This work was supported by the National Cancer Institute (R01CA138804 and R01CA188096 to BX). AHM was supported by Higher Committee for Education Development in Iraq (HCED).

References

1. Moynahan ME, Jasin M. Mitotic homologous recombination maintains genomic stability and suppresses tumorigenesis. Nature reviews. 2010; 11:196–207.
2. Xia B, Sheng Q, Nakanishi K, Ohashi A, Wu J, Christ N, et al. Control of BRCA2 cellular and clinical functions by a nuclear partner, PALB2. Mol Cell. 2006; 22:719–29. [PubMed: 16793542]
3. Sy SM, Huen MS, Chen J. PALB2 is an integral component of the BRCA complex required for homologous recombination repair. Proc Natl Acad Sci U S A. 2009; 106:7155–60. [PubMed: 19369211]
4. Zhang F, Ma J, Wu J, Ye L, Cai H, Xia B, et al. PALB2 links BRCA1 and BRCA2 in the DNA-damage response. Curr Biol. 2009; 19:524–9. [PubMed: 19268590]
5. Tischkowitz M, Xia B. PALB2/FANCN: recombining cancer and Fanconi anemia. Cancer Res. 2010; 70:7353–9. [PubMed: 20858716]
6. Antoniou AC, Casadei S, Heikkinen T, Barrowdale D, Pylkas K, Roberts J, et al. Breast-cancer risk in families with mutations in PALB2. The New England journal of medicine. 2014; 371:497–506. [PubMed: 25099575]
7. Xia B, Dorsman JC, Ameziane N, de Vries Y, Rooimans MA, Sheng Q, et al. Fanconi anemia is associated with a defect in the BRCA2 partner PALB2. Nat Genet. 2007; 39:159–61. [PubMed: 17200672]
8. Reid S, Schindler D, Hanenberg H, Barker K, Hanks S, Kalb R, et al. Biallelic mutations in PALB2 cause Fanconi anemia subtype FA-N and predispose to childhood cancer. Nat Genet. 2007; 39:162–4. [PubMed: 17200671]
9. Alter BP, Rosenberg PS, Brody LC. Clinical and molecular features associated with biallelic mutations in FANCD1/BRCA2. J Med Genet. 2007; 44:1–9. [PubMed: 16825431]
10. Bouwman P, Drost R, Klijn C, Pieterse M, van der Gulden H, Song JY, et al. Loss of p53 partially rescues embryonic development of Palb2 knockout mice but does not foster haploinsufficiency of Palb2 in tumour suppression. The Journal of pathology. 2011; 224:10–21. [PubMed: 21404276]
11. Ludwig T, Chapman DL, Papaioannou VE, Efstratiadis A. Targeted mutations of breast cancer susceptibility gene homologs in mice: lethal phenotypes of Brca1, Brca2, Brca1/Brca2, Brca1/p53, and Brca2/p53 nullizygous embryos. Genes & development. 1997; 11:1226–41. [PubMed: 9171368]
12. Hakem R, de la Pompa JL, Elia A, Potter J, Mak TW. Partial rescue of Brca1 (5–6) early embryonic lethality by p53 or p21 null mutation. Nat Genet. 1997; 16:298–302. [PubMed: 9207798]

13. Huo Y, Cai H, Teplova I, Bowman-Colin C, Chen G, Price S, et al. Autophagy opposes p53-mediated tumor barrier to facilitate tumorigenesis in a model of PALB2-associated hereditary breast cancer. Cancer discovery. 2013; 3:894–907. [PubMed: 23650262]
14. Ludwig T, Fisher P, Murty V, Efstratiadis A. Development of mammary adenocarcinomas by tissue-specific knockout of Brca2 in mice. Oncogene. 2001; 20:3937–48. [PubMed: 11494122]
15. Xu X, Wagner KU, Larson D, Weaver Z, Li C, Ried T, et al. Conditional mutation of Brca1 in mammary epithelial cells results in blunted ductal morphogenesis and tumour formation. Nat Genet. 1999; 22:37–43. [PubMed: 10319859]
16. Jonkers J, Meuwissen R, van der Gulden H, Peterse H, van der Valk M, Berns A. Synergistic tumor suppressor activity of BRCA2 and p53 in a conditional mouse model for breast cancer. Nat Genet. 2001; 29:418–25. [PubMed: 11694875]
17. Bowman-Colin C, Xia B, Bunting S, Klijn C, Drost R, Bouwman P, et al. Palb2 synergizes with Trp53 to suppress mammary tumor formation in a model of inherited breast cancer. Proc Natl Acad Sci U S A. 2013; 110:8632–7. [PubMed: 23657012]
18. Holstege H, Joosse SA, van Oostrom CT, Nederlof PM, de Vries A, Jonkers J. High incidence of protein-truncating TP53 mutations in BRCA1-related breast cancer. Cancer Res. 2009; 69:3625–33. [PubMed: 19336573]
19. Hoesel B, Schmid JA. The complexity of NF-kappaB signaling in inflammation and cancer. Molecular cancer. 2013; 12:86. [PubMed: 23915189]
20. Baud V, Karin M. Is NF-kappaB a good target for cancer therapy? Hopes and pitfalls. Nature reviews Drug discovery. 2009; 8:33–40. [PubMed: 19116625]
21. Sau A, Lau R, Cabrita MA, Nolan E, Crooks PA, Visvader JE, et al. Persistent Activation of NF-kappaB in BRCA1-Deficient Mammary Progenitors Drives Aberrant Proliferation and Accumulation of DNA Damage. Cell Stem Cell. 2016; 19:52–65. [PubMed: 27292187]
22. Nolan E, Vaillant F, Branstetter D, Pal B, Giner G, Whitehead L, et al. RANK ligand as a potential target for breast cancer prevention in BRCA1-mutation carriers. Nat Med. 2016; 22:933–9. [PubMed: 27322743]
23. Sigl V, Owusu-Boaitey K, Joshi PA, Kavirayani A, Wirnsberger G, Novatchkova M, et al. RANKL/RANK control Brca1 mutation-driven mammary tumors. Cell Res. 2016; 26:761–74. [PubMed: 27241552]
24. Anantha RW, Simhadri S, Foo TK, Miao S, Liu J, Shen Z, et al. Functional and mutational landscapes of BRCA1 for homology-directed repair and therapy resistance. Elife. 2017:6.
25. Foo TK, Tischkowitz M, Simhadri S, Boshari T, Zayed N, Burke KA, et al. Compromised BRCA1-PALB2 interaction is associated with breast cancer risk. Oncogene. 2017
26. Hartford SA, Chittela R, Ding X, Vyas A, Martin B, Burkett S, et al. Interaction with PALB2 Is Essential for Maintenance of Genomic Integrity by BRCA2. PLoS Genet. 2016; 12:e1006236. [PubMed: 27490902]
27. Simhadri S, Peterson S, Patel DS, Huo Y, Cai H, Bowman-Colin C, et al. Male fertility defect associated with disrupted BRCA1-PALB2 interaction in mice. The Journal of biological chemistry. 2014; 289:24617–29. [PubMed: 25016020]
28. Ma J, Cai H, Wu T, Sobhian B, Huo Y, Alcivar A, et al. PALB2 interacts with KEAP1 to promote NRF2 nuclear accumulation and function. Molecular and cellular biology. 2012; 32:1506–17. [PubMed: 22331464]
29. Saha T, Rih JK, Rosen EM. BRCA1 down-regulates cellular levels of reactive oxygen species. FEBS letters. 2009; 583:1535–43. [PubMed: 19364506]
30. Gorrini C, Baniasadi PS, Harris IS, Silvester J, Inoue S, Snow B, et al. BRCA1 interacts with Nrf2 to regulate antioxidant signaling and cell survival. J Exp Med. 2013; 210:1529–44. [PubMed: 23857982]
31. Bae I, Fan S, Meng Q, Rih JK, Kim HJ, Kang HJ, et al. BRCA1 induces antioxidant gene expression and resistance to oxidative stress. Cancer Res. 2004; 64:7893–909. [PubMed: 15520196]
32. Morgan MJ, Liu ZG. Crosstalk of reactive oxygen species and NF-kappaB signaling. Cell Res. 2011; 21:103–15. [PubMed: 21187859]

33. McCool KW, Miyamoto S. DNA damage-dependent NF-kappaB activation: NEMO turns nuclear signaling inside out. Immunol Rev. 2012; 246:311–26. [PubMed: 22435563]

34. Evers B, Jonkers J. Mouse models of BRCA1 and BRCA2 deficiency: past lessons, current understanding and future prospects. Oncogene. 2006; 25:5885–97. [PubMed: 16998503]

35. Rantakari P, Nikkila J, Jokela H, Ola R, Pylkas K, Lagerbohm H, et al. Inactivation of Palb2 gene leads to mesoderm differentiation defect and early embryonic lethality in mice. Hum Mol Genet. 2010; 19:3021–9. [PubMed: 20484223]

36. Domchek SM, Tang J, Stopfer J, Lilli DR, Hamel N, Tischkowitz M, et al. Biallelic deleterious BRCA1 mutations in a woman with early-onset ovarian cancer. Cancer discovery. 2013; 3:399–405. [PubMed: 23269703]

37. Sawyer SL, Tian L, Kahkonen M, Schwartzentruber J, Kircher M, et al. University of Washington Centre for Mendelian G. Biallelic mutations in BRCA1 cause a new Fanconi anemia subtype. Cancer discovery. 2015; 5:135–42. [PubMed: 25472942]

38. Freire BL, Homma TK, Funari MFA, Lerario AM, Leal AM, Velloso E, et al. Homozygous loss of function BRCA1 variant causing a Fanconi-anemia-like phenotype, a clinical report and review of previous patients. Eur J Med Genet. 2018; 61:130–3. [PubMed: 29133208]

39. Byrd PJ, Stewart GS, Smith A, Eaton C, Taylor AJ, Guy C, et al. A Hypomorphic PALB2 Allele Gives Rise to an Unusual Form of FA-N Associated with Lymphoid Tumour Development. PLoS Genet. 2016; 12:e1005945. [PubMed: 26990772]

40. Nan J, Du Y, Chen X, Bai Q, Wang Y, Zhang X, et al. TPCA-1 is a direct dual inhibitor of STAT3 and NF-kappaB and regresses mutant EGFR-associated human non-small cell lung cancers. Mol Cancer Ther. 2014; 13:617–29. [PubMed: 24401319]

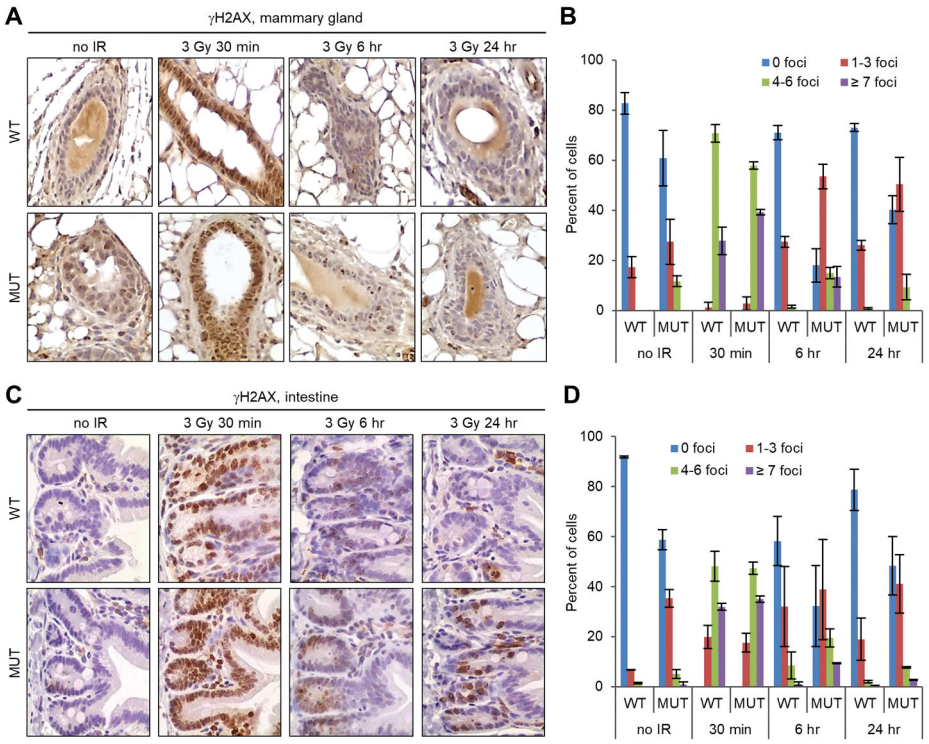

Figure 1.

Endogenous DNA damage and DSB repair capacity in wt and *Palb2* mutant mice. (**A,B**) Representative IHC images (**A**) and quantification (**B**) of γH2AX foci formation in the mammary gland before and after 3 Gy of IR. (**C,D**) Representative IHC images (**C**) and quantification (**D**) of γH2AX foci formation in the intestine before and after 3 Gy of IR. Data shown are means ± standard deviations (SD) from 2 independent experiments.

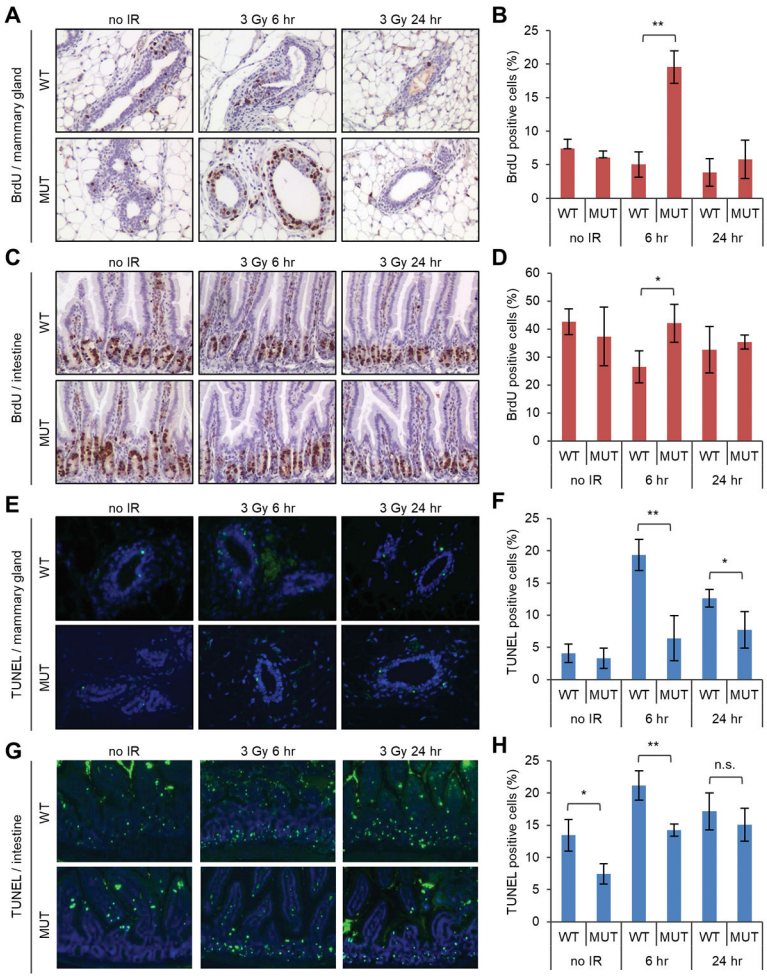

Figure 2.

DNA synthesis and apoptosis in wt and *Palb2* mutant mice before and after radiation. (**A,B**) Representative IHC images of BrdU incorporation (**A**) and quantification of BrdU-positive cells (**B**) in the mammary gland. (**C,D**) Representative IHC images of BrdU incorporation (**C**) and quantification of BrdU-positive cells (**D**) in the intestine. (**E,F**) Representative images of TUNEL staining (**E**) and quantification of TUNEL-positive cells (**F**) in the mammary gland. (**G,H**) Representative images of TUNEL staining (G) and quantification of TUNEL-positive cells (H) in the intestine. The mice were treated with 3 Gy of IR in all panels. BrdU labeling was for 30 min immediately before tissue collection at each time point. Data shown are means ± standard deviations (SD) from 3 independent experiments. *, $p<0.05$; **, $p<0.01$.

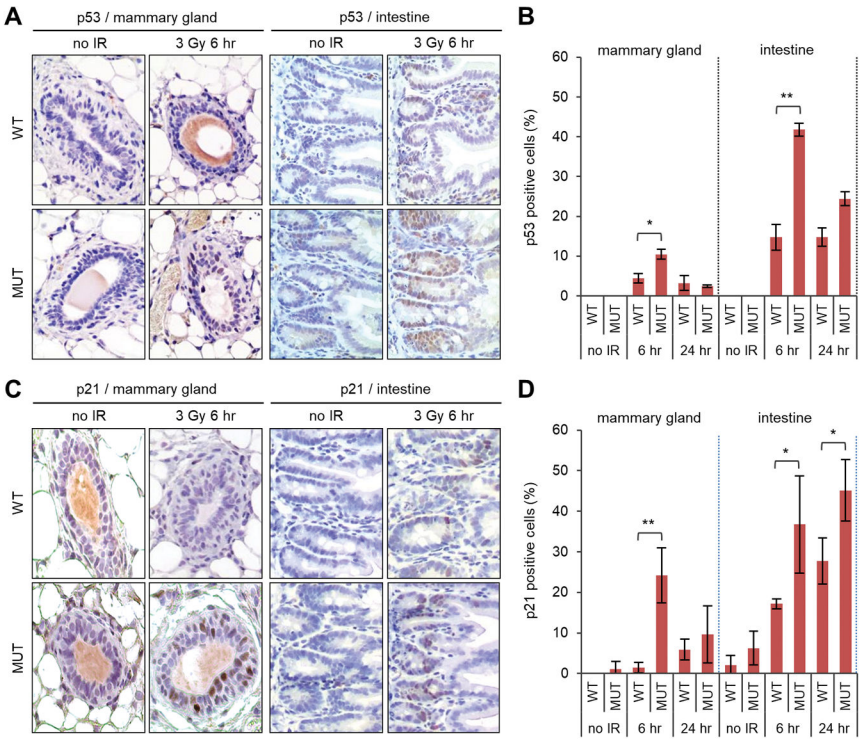

Figure 3.

Levels of p53 and p21 in wt and *Palb2* mutant mice before and after radiation. (**A,B**) Representative p53 IHC images (**A**) and quantification of p53-positive cells (**B**) in the mammary gland before and after 3 Gy of IR. (**C,D**) Representative p21 IHC images (**C**) and quantification of p21-positive cells (**D**) in the intestine before after 3 Gy of IR. Data shown are means ± SD from 2 independent experiments for p53 and 3 independent experiments for p21. *, $p<0.05$; **, $p<0.01$.

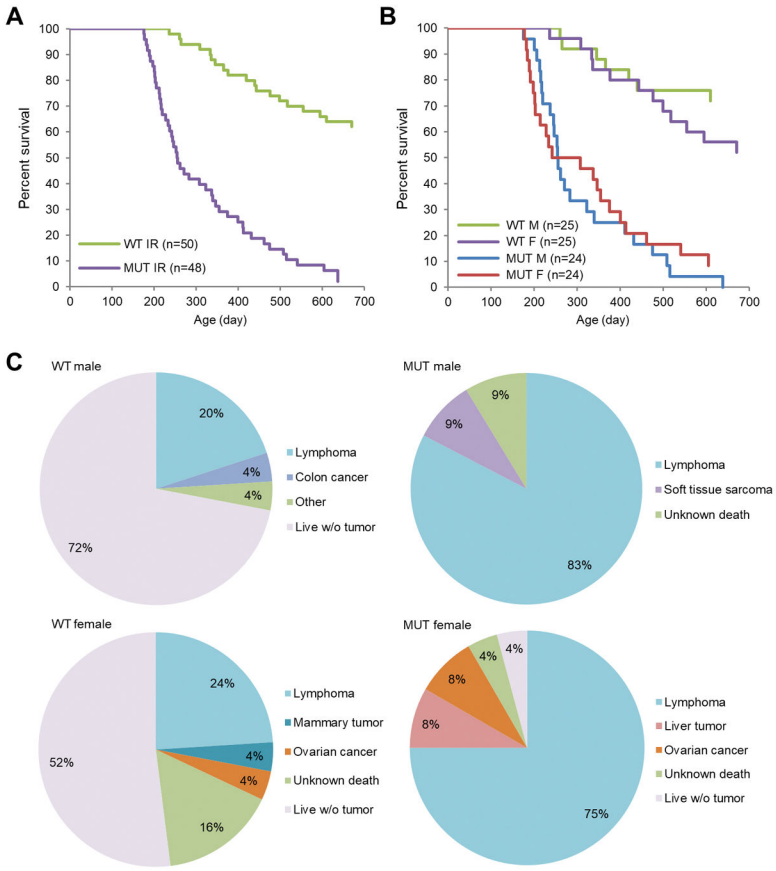

Figure 4.

Radiation-induced tumor development in wt and *Palb2* mutant mice. (**A,B**) Kaplan-Meier curves of overall survival of wt and mutant mice after radiation with males and females combined (**A**) or separated (**B**). (**C**) Spectra of tumor development in wt and mutant males and females after radiation.

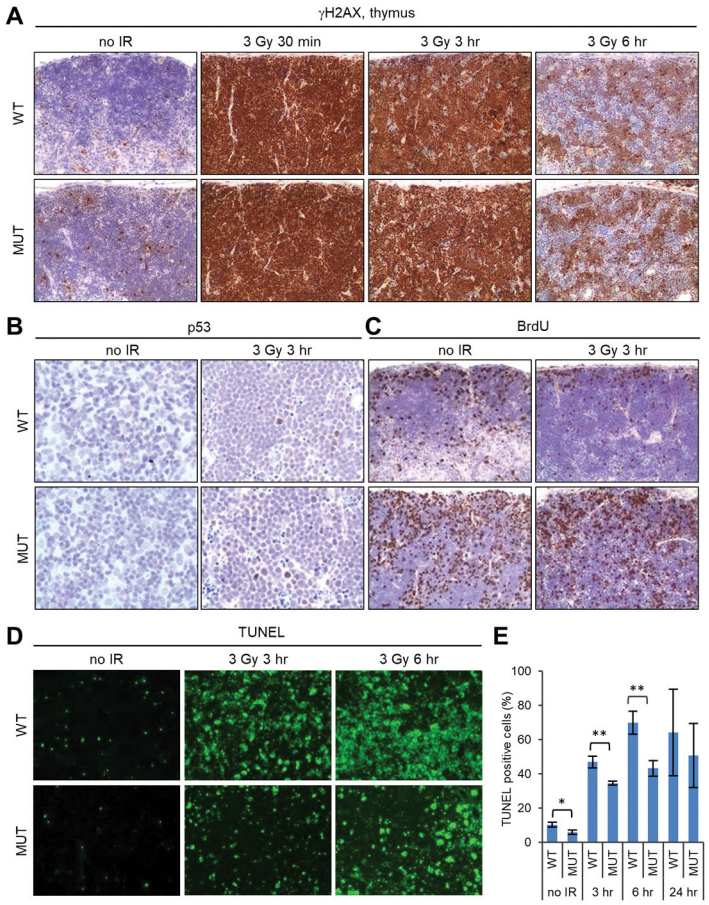

Figure 5.

DNA damage response in the thymus of wt and *Palb2* mutant mice. (**A-C**) Representative IHC images of γH2AX (**A**), p53 (**B**) and BrdU incorporation (**C**) before and after 3 Gy of IR. (**D,E**) Representative images of TUNEL staining and quantification of TUNEL-positive cells (**E**) before and after 3 Gy of IR. Data shown are means ± SD from 3 independent experiments. *, $p<0.05$; **, $p<0.01$.

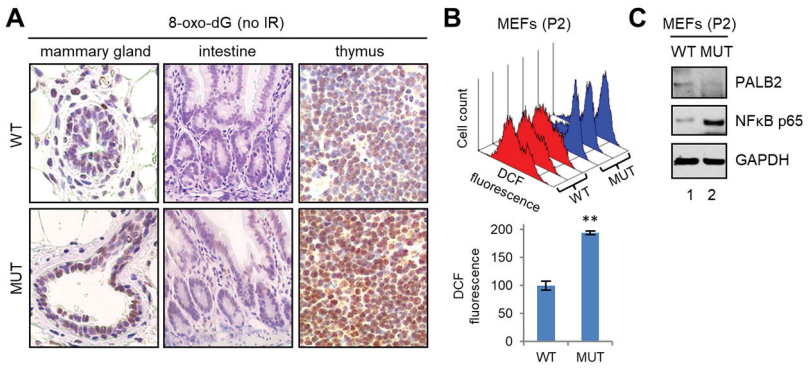

Figure 6.

Evidence of increased oxidative stress in *Palb2* mutant mice. (**A**) Representative IHC images of 8-oxo-dG in the mammary gland, intestine and thymus of wt and mutant mice. (**B**) ROS levels in wt and mutant primary MEFs at passage 2. Top panel, DCF fluorescence histograms of 3 pairs of wt (red) and mutant (blue) cells; lower panel, combined DCF fluorescence values of the 3 pairs of cells. (**C**) Representative western blots showing PALB2 and NFκB p65 levels in wt and *Palb2* mutant MEFs.

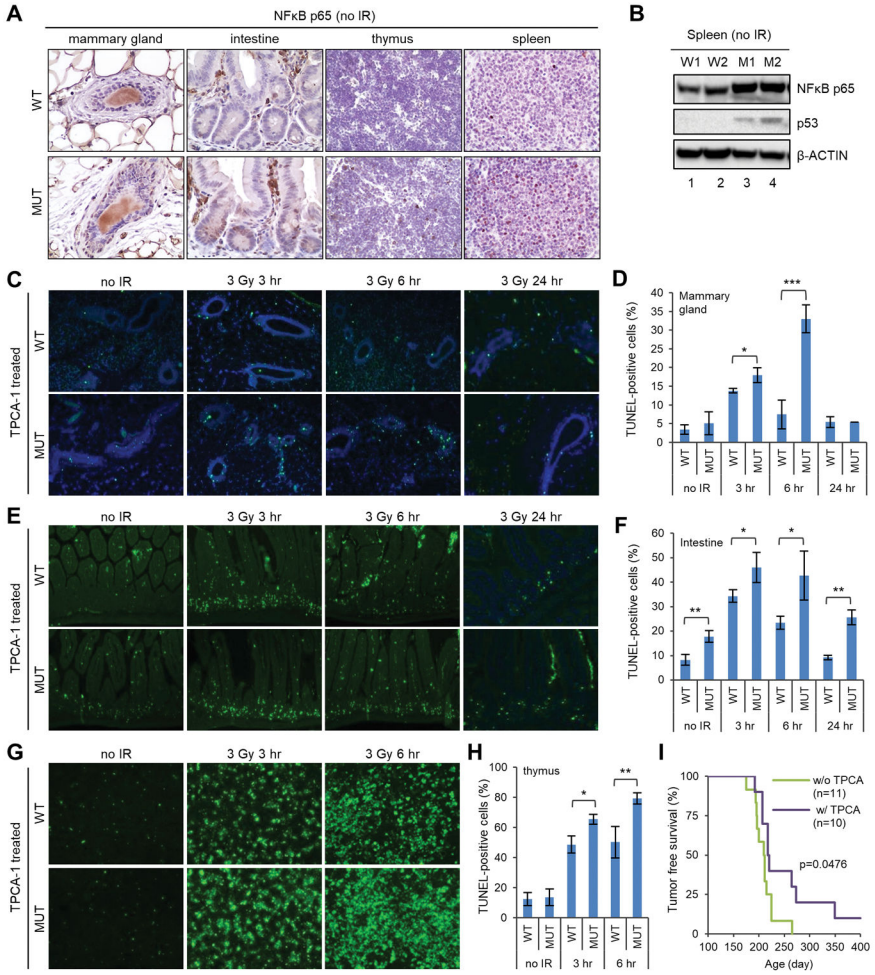

Figure 7.

Evidence for a role of NFκB in apoptosis and tumor development in *Palb2* mutant mice after radiation. (**A**) Representative IHC images of NFκB (p65) in the mammary gland, intestine, thymus and spleen of wt and mutant mice. (**B**) Western blots showing the amounts of NFκB (p65) and p53 in the spleen of wt and mutant mice. Two pairs of mice (W1, W2 and M1, M2, respectively) were tested. (**C,D**) Representative TUNEL staining images (**C**) and quantification of TUNEL-positive cells (**D**) in the mammary gland of TPCA-1 treated wt and mutant mice before and after 3 Gy of radiation. (**E,F**) Representative TUNEL staining images (**E**) and quantification of TUNEL-positive cells (**F**) in the intestine of TPCA-1 treated mice before and after 3 Gy of radiation. (**G,H**) Representative TUNEL staining images (**G**) and quantification of TUNEL-positive cells (**H**) in the thymus of TPCA-1 treated mice before and after 3 Gy of radiation. For all TUNEL experiments, results shown are means ± SD from 3 independent experiments. *, $p<0.05$; **, $p<0.01$. (**I**) Kaplan-Meier tumor-free survival curves of TPCA-1 untreated and treated *Palb2* mutant mice after 3 × 2 Gy of radiation. P value is calculated by log-rank analysis using GraphPad Prism7.